NuSTAR Detection of X-Ray Heating Events in the Quiet Sun — **Source link** ⬈

Matej Kuhar, Matej Kuhar, Säm Krucker, Säm Krucker ...+7 more authors

Institutions: ETH Zurich, University of Applied Sciences and Arts Northwestern Switzerland FHNW, University of California, Berkeley, University of Minnesota ...+4 more institutions

Related papers:
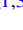
- NuSTAR hard X-ray observation of a sub-A class solar flare

- Microflare Heating of a Solar Active Region Observed with NuSTAR, Hinode/XRT, and SDO/AIA

- The Atmospheric Imaging Assembly (AIA) on the Solar Dynamics Observatory (SDO)

- The multi-thermal emission in solar active regions

- THE NUCLEAR SPECTROSCOPIC TELESCOPE ARRAY (NuSTAR) HIGH-ENERGY X-RAY MISSION

NuSTAR Detection of X-Ray Heating Events in the Quiet Sun

Matej Kuhar[1,2] , Säm Krucker[1,3], Lindsay Glesener[4] , Iain G. Hannah[5] , Brian W. Grefenstette[6] , David M. Smith[7] ,
Hugh S. Hudson[3,5] , and Stephen M. White[8]

[1] University of Applied Sciences and Arts Northwestern Switzerland, Bahnhofstrasse 6, 5210 Windisch, Switzerland
[2] Institute for Particle Physics and Astrophysics, ETH Zürich, 8093 Zürich, Switzerland
[3] Space Sciences Laboratory, University of California, Berkeley, CA 94720-7450, USA
[4] School of Physics and Astronomy, University of Minnesota—Twin Cities, Minneapolis, MN 55455, USA
[5] SUPA School of Physics & Astronomy, University of Glasgow, Glasgow G12 8QQ, UK
[6] Cahill Center for Astrophysics, 1216 East California Boulevard, California Institute of Technology, Pasadena, CA 91125, USA
[7] Physics Department and Santa Cruz Institute for Particle Physics, University of California, Santa Cruz, 1156 High Street, Santa Cruz, CA 95064, USA
[8] Air Force Research Laboratory, Albuquerque, NM, USA

Abstract

The explanation of the coronal heating problem potentially lies in the existence of nanoflares, numerous small-scale heating events occurring across the whole solar disk. In this Letter, we present the first imaging spectroscopy X-ray observations of three quiet Sun flares during the *Nuclear Spectroscopic Telescope ARray* (*NuSTAR*) solar campaigns on 2016 July 26 and 2017 March 21, concurrent with the *Solar Dynamics Observatory*/Atmospheric Imaging Assembly (*SDO*/AIA) observations. Two of the three events showed time lags of a few minutes between peak X-ray and extreme ultraviolet emissions. Isothermal fits with rather low temperatures in the range 3.2–4.1 MK and emission measures of $(0.6–15) \times 10^{44} \, \mathrm{cm^{-3}}$ describe their spectra well, resulting in thermal energies in the range $(2–6) \times 10^{26}$ erg. *NuSTAR* spectra did not show any signs of a nonthermal or higher temperature component. However, as the estimated upper limits of (hidden) nonthermal energy are comparable to the thermal energy estimates, the lack of a nonthermal component in the observed spectra is not a constraining result. The estimated *Geostationary Operational Environmental Satellite* (*GOES*) classes from the fitted values of temperature and emission measure fall between 1/1000 and 1/100 A class level, making them eight orders of magnitude fainter in soft X-ray flux than the largest solar flares.

Key words: Sun: flares – Sun: particle emission – Sun: X-rays, gamma rays

1. Introduction

The explanation of how the corona keeps its temperature of a few million Kelvin, termed the "coronal heating problem," has eluded scientists for decades. Because solar flares release energy and heat ambient plasma, it is argued that they may provide (at least a part of) the needed energy to sustain coronal temperatures.

Solar flares follow a negative power-law frequency distribution with increasing energy, with a power-law index ∼2 (e.g., Hudson 1991; Hannah et al. 2008). A flat distribution, with a power-law index below 2, implies that smaller events do not dominate the energy released in flares. As the largest flares do not occur frequently enough to heat the solar corona, it has been instead argued that smaller-scale reconnection events could have a steeper frequency distribution, providing the needed energy input due to large numbers. Parker (1988) introduces the term *nanoflares* for such events, with energies speculated to be of the order of 10^{24} erg or less, as estimated from ultraviolet fluctuations within active regions (Porter et al. 1984). This triggered many theoretical studies on the role of small-scale events in coronal heating (e.g., Walsh & Ireland 2003; Klimchuk 2006; Browning et al. 2008; Tajfirouze & Safari 2012; Guerreiro et al. 2015, 2017).

Parker's basic magnetic energy releases, however, are yet to be confirmed observationally, most probably due to their modest sizes and energies, combined with sensitivity limitations of present solar instruments. So far, only measurements of individual events down to ∼10^{24} erg (at the "high-energy" end of Parker's estimate) have been performed, while less energetic nanoflares could have even smaller energies and should form an ensemble of indistinguishable reconnection and heating processes that make the solar corona. In addition to searches for nanoflares in soft X-rays (SXRs; e.g., Shimizu & Tsuneta 1997; Katsukawa & Tsuneta 2001; Terzo et al. 2011), the most complete statistical study of microflares in hard X-rays is by Hannah et al. (2008), using six years of *Reuven Ramaty High Energy Solar Spectroscopic Imager* (*RHESSI*; Lin et al. 2002) data and including more than 25,000 microflares. However, because *RHESSI* is sensitive to flares with temperatures above ∼10 MK and emission measures (EMs) above $10^{45} \, \mathrm{cm^{-3}}$, the events included in the above study are much larger and more energetic than the nanoflares proposed by Parker (1988). Another distinctive feature is that *RHESSI* observes microflares only from active regions, while nanoflares should occupy the whole solar disk. Quiet Sun (QS) flares, on the other hand, have been observed only in SXR and extreme ultraviolet (EUV) narrow-band filter observations (e.g., Krucker et al. 1997; Krucker & Benz 1998; Aschwanden et al. 2000; Parnell & Jupp 2000). These brightenings have been found to occur on the magnetic network of the QS, corroborating the magnetic energy releases as their drivers. Radio events in the GHz range associated with the EUV brightenings have been speculated to be signatures of nonthermal electrons accelerated during the energy release process (Benz & Krucker 1999). Their spectroscopic X-ray signatures, however, are too faint for the state-of-the-art solar X-ray instruments. Therefore, in order to confirm Parker's nanoflare scenario of coronal heating, it is crucial to perform sensitive imaging spectroscopy X-ray observations of small-scale events across the whole solar disk.
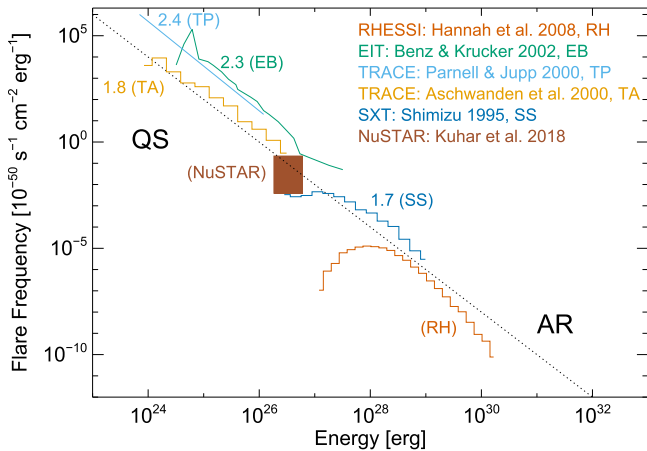
Figure 1. Flare frequency distribution vs. energy from various X-ray and EUV studies. *NuSTAR* observations analyzed in this Letter are presented as the brown rectangle. Note that the presented studies used data from different phases of the solar cycle, making comparisons of the flare occurrence between them difficult. The dotted line shows one frequency distribution with a power-law index of 2 to guide the eye. Taken from Hannah et al. (2011) and adapted to include our results.

The *Nuclear Spectroscopic Telescope ARray* (*NuSTAR*) is a focusing optics hard X-ray telescope launched in 2012 and operating in the energy range 3–79 keV (Harrison et al. 2013). Even though it is not solar-dedicated, it is capable of observing the Sun (Grefenstette et al. 2016), providing much higher sensitivity compared to indirect imaging telescopes such as *RHESSI*. It can therefore bridge the gap toward imaging spectroscopy in X-rays of small-scale heating events in the QS, and provide the opportunity to search for nonthermal signatures in them. This can be seen in Figure 1, where we show flare frequency distributions from various X-ray and EUV studies of microflares and QS brightenings (Shimizu 1995; Aschwanden et al. 2000; Parnell & Jupp 2000; Benz & Krucker 2002; Hannah et al. 2008). The plot can be divided into two segments: the left one shows EUV observations of flares in the QS, and the right one shows X-ray observations of microflares from active regions. QS *NuSTAR* observations from this study are shown by the brown box.

In this Letter, we present the first spectroscopically resolved X-ray measurements of QS flares. *NuSTAR* observations of QS heating events are described in Section 2. Data analysis and spectral fitting of the events are found in Section 3, while the discussion on this and possible future studies is presented in Section 4.

2. Observations

The data analyzed in this Letter were obtained in *NuSTAR* solar campaigns carried out on 2016 July 26 and 2017 March 21.[9] Three QS events were observed during 1.5 hr of analyzed *NuSTAR* observations, one on 2016 July 26 and two others on 2017 March 21. They will be referred to as flares 1, 2, and 3 in the future sections, based on their chronological order.

Figure 2 shows the spatial structure and time evolution for each of the events. The left panels show Atmospheric Imaging Assembly (AIA; Lemen et al. 2012) 335 Å images of the part of the solar disk where the events occurred, together with the

---

30%, 50% and 70% *NuSTAR* contours in red. *NuSTAR* images have been shifted to match the flare locations in the AIA images in order to accommodate for uncertainties in absolute pointing (Grefenstette et al. 2016). A zoomed-in image of each event is shown in the inset. The right panels show the time evolution of *NuSTAR* flux above 2.0 keV, as well as the time evolution of AIA EUV channels. All fluxes are background-subtracted, where background is defined as the lowest emission time frame during the pre-event phase.

2.1. Time Evolution

The time profiles of flares generally reveal different behaviors for the thermal and nonthermal X-ray component. Nonthermal emissions are most prominently observed during the rise phase of the thermal emission (impulsive phase) and can show several peaks with durations from a minute down to a subsecond timescale (e.g., Aschwanden et al. 1995). The main thermal emission evolves more gradually, with a time profile often similar to the integrated nonthermal flux (the so-called "Neupert effect"; Neupert 1968). (Hard) X-ray peaks that occur before the thermal peak (seen in SXR and/or EUV) are therefore often interpreted as a signature of nonthermal emission (Veronig et al. 2005), but such a classification is not conclusive. Time lags between X-ray and EUV emission can also be produced by the different temperature sensitivity of X-ray and EUV observations: the X-ray peak is produced by the flare-heated plasma, which then cools to lower temperatures visible in EUV. To resolve the ambiguities present in the time evolution of X-ray and EUV emission, a spectral analysis is required. In the following, we discuss the time evolution of the individual events focusing on potential nonthermal signatures, followed by the spectral analysis in Section 3.

Flare 1 shows an intriguing time evolution with two distinctive X-ray peaks, while flares 2 and 3 have one broad peak dominating both the X-ray and EUV evolution. Flare 3 shows simultaneous X-ray and EUV peaks; this is in contrast to flares 1 and 2, which show a time lag of a few minutes between peak X-ray and EUV emissions. The rise of the EUV emission, as well as the decay, is slower than in X-rays for all flares. In order to interpret the observed relative timing, it is important to consider the difference in temperature responses between *NuSTAR* and AIA. *NuSTAR* has a steeply increasing response toward higher temperatures between 1 and 10 MK, making it sensitive primarily to the highest temperature plasma in this range. The AIA temperature response, on the other hand, is much broader and the resulting flux represents contributions from plasma at various temperatures. The time evolution of flare 2 can be explained by the process of plasma cooling, where *NuSTAR* peaks first, followed by the AIA channels according to their temperature sensitivity. The other events are more complex, and only a detailed temporal and spatial differential emission measure analysis might allow us to understand their complicated time evolution; this is outside the scope of this Letter. The spectral analysis presented in Section 3 further addresses the question of whether the delays between *NuSTAR* and AIA peaks imply nonthermal emission in these events.

2.2. Flare Locations and Morphology

Flare locations and morphologies can be found in the insets of the left panels in Figure 2. Flare 1 evidenced an ejection of
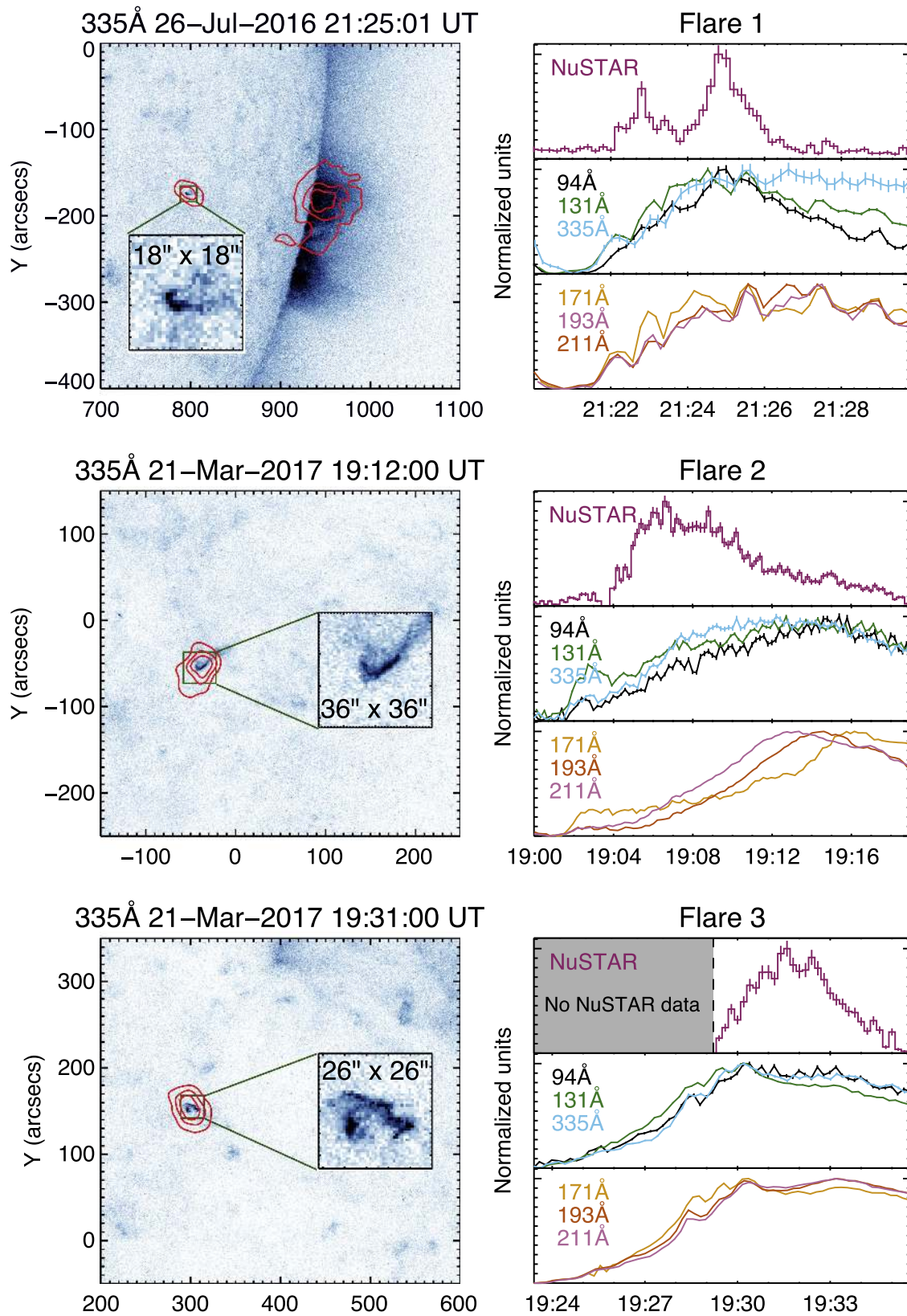
Figure 2. Overview plots of the three QS flares. Left panels: $400'' \times 400''$ AIA 335 Å images of the events, together with zoomed-in images of the event morphology in the insets. The 30%, 50%, and 70% contours of maximum *NuSTAR* emission are shown in red. Right panels: background-subtracted time evolution of the flaring region and flux uncertainties in the combined flux of *NuSTAR* focal plane modules A and B above 2.0 keV, together with AIA 94, 131, 335, 171, 193, and 211 Å channels. Error bars in 171, 193, and 211 Å channels are smaller than the line thickness.

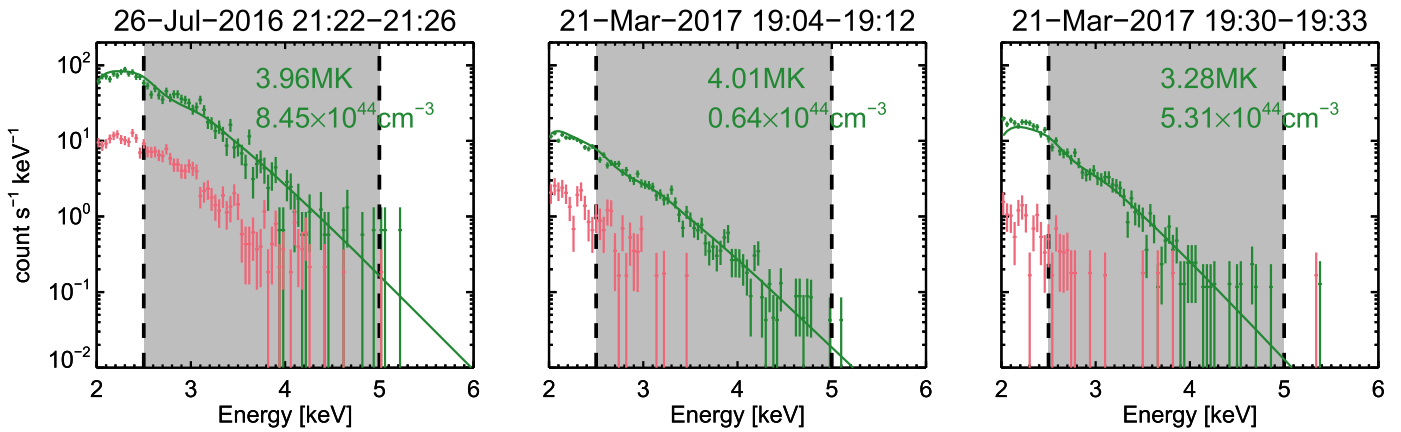**Figure 3.** *NuSTAR* spectra of the observed QS flares. Spectra with best isothermal fits for *NuSTAR* focal plane modules A and B combined is shown in dark green, while the background counts are shown in pink. The energy range 2.5–5.0 keV used for spectral fitting is denoted by the gray area between the vertical dashed lines.

Table 1
QS Flare Parameters

Flare	Date [yyyy mm dd]	Time [hh:mm]	Location [x, y]	Area [arcsec^2]	Temperature [MK]	Emission Measure [10^{44} cm^{-3}]	Density [10^9 cm^{-3}]	Energy 10^{26} [erg]	*GOES* Class [A]
1	2016 Jul 26	21:24	[795, −175]	38	$3.96^{+0.05}_{-0.40}$	$8.5^{+6.3}_{-0.9}$	$3.0^{+1.0}_{-0.2}$	$4.5^{+1.5}_{-0.7}$	0.01
2	2017 Mar 21	19:04	[−40, −55]	75	$4.02^{+0.05}_{-0.22}$	$(2\times)\,0.64^{+0.22}_{-0.08}$	$(\sqrt{2}\times)\,0.51^{+0.08}_{-0.03}$	$(\sqrt{2}\times)\,2.1^{+0.4}_{-0.2}$	$(2\times)\,0.0009$
3	2017 Mar 21	19:30	[300, 150]	85	$3.28^{+0.13}_{-0.06}$	$5.3^{+1.8}_{-1.8}$	$1.3^{+0.2}_{-0.3}$	$5.4^{+1.1}_{-1.1}$	0.003

material during the impulsive phase, seen in all AIA channels. It occurred in the QS. Flare 2 was a part of a long-lasting elongated structure located in proximity to the solar disk center, with the flaring area that was just a fraction of the whole structure. The morphology of the structure is reminiscent of heated flare loops. Flare 3 was a short-duration event that, like Flare 1, was not associated with any kind of X-ray or EUV structure. However, it showed an even more complex structure than flare 1. The March events were clearly associated with the QS magnetic network structures, while the association is not as clear for the July event. However, this might be due to its proximity to the solar disk, where the line of sight effects could mask the signal.

To conclude, in spite of their modest sizes and emission, the observed events show very complex spatial and temporal morphologies and therefore cannot be described as "elementary" energy releases proposed by Parker. They were not part of active regions, and are therefore classified as QS events.

3. Data Analysis

3.1. Spectra

NuSTAR allows us to produce spectra for any time range, energy range (above 2.5 keV), and area. For our study, we use circular regions with a diameter of 55″ (a value close to *NuSTAR*'s half power diameter) at each flare's location. Integration times were chosen individually for each flare so that the majority of X-ray emission is included (presented spectra are flare-integrated) and are equal to 4, 8, and 3 minutes for flares 1, 2, and 3, respectively. To perform spectral fitting in XSPEC (Arnaud 1996), *NuSTAR* spectra and response matrix files were obtained using standard *NuSTAR* data analysis software.[10] In the following, we perform simultaneous fitting in XSPEC on the data from both focal plane modules, which are

then combined to display the results shown in Figure 3 and Table 1. We fit an isothermal (APEC in the XSPEC package, using abundances from Feldman et al. 1992) plus a fixed background model between 2.5 and 5.0 keV, where we estimate the background as a two-minute integrated emission in the pre-flare phase, mostly consisted of ghost-rays (photons from sources outside the field of view).

NuSTAR spectra are shown in Figure 3. The fits give temperatures of $3.96^{+0.05}_{-0.40}$, $4.01^{+0.05}_{-0.22}$, and $3.28^{+0.13}_{-0.06}$ MK, while their EMs lie in the range 5.6×10^{43}–1.5×10^{45} cm^{-3}. These values of temperature and emission measure place our events just in between the active region microflares and the QS events analyzed previously in the EUV. Our events are at or slightly below the *NuSTAR* detection limit as derived from previous observations with lower livetime and much stronger ghost-ray signal (Marsh et al. 2017). Here we note that the estimated EM for flare 2 is probably a lower limit, as we estimate that up to 50% of the total flare emission might not be accounted for in our fits. This is due both to its proximity to the chip gap and a lot of changes in the combination of *NuSTAR* camera head units used for pointing, which resulted in many (abrupt) changes in the estimated flare location. This probably has no effect on the temperature estimates, but the actual EM is likely a factor of 2 larger than the one reported. This is also shown in Table 1, with a factor 2 in parenthesis for parameters affected by this effect. The above-reported temperatures and EMs place the observed events in the estimated range between 1/1000 and 1/100 *GOES* A-class equivalents, or between 7 and 8 classes fainter than the largest solar flares.

It is interesting to note the low temperatures of *NuSTAR* QS flares. While *RHESSI* is designed to observe flares with temperatures above 10 MK, *NuSTAR* is able to observe lower temperatures due to its higher low-energy sensitivity. However, because *NuSTAR*'s sensitivity also increases with increasing temperature, the fit-determined temperatures are the highest temperatures (as weighted by emission measure) present in the

---

[10] https://heasarc.gsfc.nasa.gov/docs/nustar/analysis/

events. Therefore, it seems that QS flares reach only modest temperatures compared to those generally observed in regular active region flares. The only other possibility is that hotter QS events have significantly lower EMs, making them hard to observe even with *NuSTAR*.

3.2. Thermal Energy Content

We use the standard approach of estimating total thermal flare energy content from the flare plasma at the highest temperature as derived from *NuSTAR* spectra. This approach assumes that any cooler plasma, such as that observed in the EUV, is a result of the cooling process. Wright et al. (2017) estimated that this approximation could be up to ~30% different from the estimate from a complete, differential emission measure analysis of multithermal plasma in an active region microflare observed with *NuSTAR* and AIA. In this approximation, the thermal energy content of an event with temperature T, emission measure EM, and volume V is given by the formula (e.g., Hannah et al. 2008)

$$E_{\rm th} \sim 3NkT = 3kT\sqrt{\rm EM \cdot V}. \qquad (1)$$

To estimate upper and lower limits on the total thermal energy content, we use the combination of maximum and minimum of possible values for temperature and EM as given by the fits.

Because the observed QS flares are not spatially resolved with *NuSTAR*, we estimate flare volumes as the area of flaring 335 Å pixels (other channels have similar flaring areas) to the power of 3/2. As *NuSTAR* is only sensitive to the hottest plasma, while AIA is sensitive to a broader range of temperatures, this estimate provides an upper limit for the actual volume and, consequentially, a lower limit for the density and an upper limit for the thermal energy content (an overestimate up to a factor of 5 in the thermal energy content is possible). Density estimates can be calculated with the formula $n = \sqrt{\rm EM/V}$ and fall in the range $(0.5-4) \times 10^9\,{\rm cm}^{-3}$. These values are similar to those derived from SXR QS flares by Krucker et al. (1997) $((1-5) \times 10^9\,{\rm cm}^{-3})$, but larger than densities derived from EUV QS events by Aschwanden et al. (2000) $((0.1-0.5) \times 10^9\,{\rm cm}^{-3})$. We calculate the following thermal energy contents for flares 1, 2, and 3: $(3.8-6.0) \times 10^{26}$, $(1.8-2.5) \times 10^{26}$, and $(3.9-5.9) \times 10^{26}$ erg. These values are about five orders of magnitude smaller than in largest solar flares.

3.3. Nonthermal Emission

There is no evidence for a high temperature or a nonthermal component in the spectra presented in Figure 3, and no counts above ~5 keV are observed. By setting an upper limit for the potentially hidden nonthermal contribution, we estimate an upper limit of the energy in nonthermal electrons in the same way as has been in done in Wright et al. (2017) and taking flare 1 as an example. The addition of a hidden nonthermal component with a low-energy cutoff at 5 keV and a power-law index of 7 still reproduces the observed spectrum well, giving undetectable signal above the cutoff. The estimated upper limit of the nonthermal energy equals ~5×10^{26} erg, a value within the uncertainties of the estimated thermal energy. Hence, the non-detection of a nonthermal component in the observed spectra is not a constraining result, with its upper limits still consistent with the observed heating.
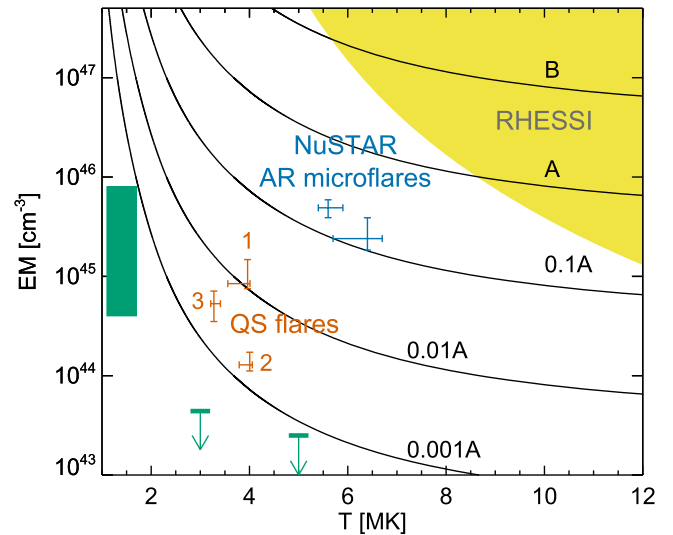

Figure 4. Three analyzed events (orange) in the *T*–EM parameter space, together with two active region microflares (blue) observed in previous *NuSTAR* solar campaigns. The QS network flares observed with *Yohkoh*/Soft X-Ray Telescope (SXT; Krucker et al. 1997) are depicted with the green box, together with the estimated upper limits in the temperature range of our QS events. *GOES-13* classes between 0.001A and B are shown by isocurves. The part of the parameter space observable by *RHESSI* is shown in yellow.

4. Discussion and Conclusions

In this Letter, we analyzed three QS flares observed in X-rays above 2.0 keV with *NuSTAR*. We were able to measure their X-ray spectra for the first time and derive flare peak temperatures (see Table 1 for the summary of the derived parameters). Despite their modest sizes and X-ray emission, these events show very complex spatial morphologies in the EUV. They are therefore not elementary energy releases and still much larger than Parker's idea of nanoflares.

Figure 4 shows our events in the *T*–EM parameter space, together with two *NuSTAR* active region microflares observed in previous campaigns (Glesener et al. 2017; Wright et al. 2017). The green box represents SXR QS events from Krucker et al. 1997, showing that they reach even lower temperatures and are below the sensitivity limits of our current observations. The isocurves show *GOES* classes, while the yellow area denotes the parameter space observable by *RHESSI*. For flares with temperatures between 3 and 4 MK as discussed here, *RHESSI* is sensitive to EMs above ~$10^{49}\,{\rm cm}^{-3}$, meaning that we gained at least four orders of magnitude in EM sensitivity compared to *RHESSI*. Another interesting result are the rather low temperatures of up to ~4 MK, indicating that QS flares might be reaching lower temperatures than the ones generally observed in active region flares.

In contrast to hints coming from the time evolution of *NuSTAR* and AIA fluxes, *NuSTAR* spectra did not show any sign of a high-temperature or a nonthermal component. However, as the estimated upper limits of energy in the hidden nonthermal component are comparable to the calculated thermal energies, the lack of a nonthermal component is not a strong diagnostic result.

What follows next? Solar observations with *NuSTAR* started in 2014 September and have been carried out sporadically every few months, depending on science questions addressed and solar conditions, giving 12 observations in total at the time

of writing. Taking into account the EUV QS flare frequency distribution (Figure 1), we expect a few QS events of energies $\sim 10^{26}$ erg per hour within the *NuSTAR* field of view. This is roughly in agreement with our observations of three events in 1.5 hr of data. We overplot our observations in the frequency distribution plot in Figure 1 as a brown shaded box. The height of the box represents uncertainty in determining the number of events in the low-statistics regime following the approach of Gehrels (1986) and taking the conservative 99% confidence interval, while the width of the box represents the thermal energy range of our events.

As the Sun's activity decreases toward solar minimum in 2019/2020, we expect progressively better conditions for observations of QS flares. We can get an estimate of this by inspecting detector livetimes and count rates of the observed events. The data for flare 3 are taken here as an example. We emphasize the following points that will improve the sensitivity during optimal observing conditions.

1. Livetime could improve by a factor of $1/0.59 \approx 1.7$ in periods of low solar activity.
2. *NuSTAR* detected 900 counts above 2.5 keV during the event, with background contributing $\sim 3\%$ of the emission (see Figure 3). In the absence of any activity during solar minimum observations, we expect ghost-rays to largely disappear, reducing the background emission to values that are close to zero. The spectral analysis could then be performed with many fewer counts than we observed for flare 3; an improvement in sensitivity of up to a factor of 10 seems feasible.
3. Counts below 2.5 keV, where *NuSTAR* calibration is inaccurate due to threshold uncertainties and ghost-ray influence is strongest, have not been used for spectral fitting. In the absence of ghost-rays, however, using counts down to 1.6 keV can be used for flare detection. While spectral fitting will be affected by uncertainties in calibration below 2.5 keV, we might still get acceptable energy estimates. Moving the lower energy limit down to 1.6 keV would increase our statistics by a factor of four.

Combining these factors would lead to a sensitivity increase of a factor of ~ 70. Assuming the same flare temperature, *NuSTAR* could observe QS flares with EMs of $\sim 8 \times 10^{42}$ cm^{-3} and thermal energies of $\sim 7 \times 10^{25}$ erg. Assuming the flare frequency distribution index of 2, we would expect ~ 15 events per hour within the *NuSTAR* field of view. Of course, smaller events might have lower temperatures and/or different areas than the events presented here, making if difficult to estimate a lower limit of the energy content that can be reached. Even if we do not reach such low energies, observing even a few events per hour would be a significant step forward to a statistical study, which would provide further insights into the energy content and heating processes in the faintest impulsive events on the Sun.

ORCID iDs

Matej Kuhar https://orcid.org/0000-0002-7210-180X
Lindsay Glesener https://orcid.org/0000-0001-7092-2703
Iain G. Hannah https://orcid.org/0000-0003-1193-8603
Brian W. Grefenstette https://orcid.org/0000-0002-1984-2932
David M. Smith https://orcid.org/0000-0002-0542-5759
Hugh S. Hudson https://orcid.org/0000-0001-5685-1283

References

Arnaud, K. A. 1996, adass V, 101, 17
Aschwanden, M. J., Schwartz, R. A., & Alt, D. M. 1995, ApJ, 447, 923
Aschwanden, M. J., Tarbell, T. D., Nightingale, R. W., et al. 2000, ApJ, 535, 1047
Benz, A. O., & Krucker, S. 1999, A&A, 341, 286
Benz, A. O., & Krucker, S. 2002, ApJ, 568, 413
Browning, P. K., Gerrard, C., Hood, A. W., Kevis, R., & van der Linden, R. A. M. 2008, A&A, 485, 837
Feldman, U., Mandelbaum, P., Seely, J. F., Doschek, G. A., & Gursky, H. 1992, ApJS, 81, 387
Gehrels, N. 1986, ApJ, 303, 336
Glesener, L., Krucker, S., Hannah, I. G., et al. 2017, ApJ, 845, 122
Grefenstette, B. W., Glesener, L., Krucker, S., et al. 2016, ApJ, 826, 20
Guerreiro, N., Haberreiter, M., Hansteen, V., & Schmutz, W. 2015, ApJ, 813, 61
Guerreiro, N., Haberreiter, M., Hansteen, V., & Schmutz, W. 2017, A&A, 603, A103
Hannah, I. G., Christe, S., Krucker, S., et al. 2008, ApJ, 677, 704
Hannah, I. G., Hudson, H. S., Battaglia, M., et al. 2011, SSRv, 159, 263
Harrison, F. A., Craig, W. W., Christensen, F. E., et al. 2013, ApJ, 770, 103
Hudson, H. S. 1991, SoPh, 133, 357
Katsukawa, Y., & Tsuneta, S. 2001, ApJ, 557, 343
Klimchuk, J. A. 2006, SoPh, 234, 41
Krucker, S., & Benz, A. O. 1998, ApJL, 501, L213
Krucker, S., Benz, A. O., Bastian, T. S., & Acton, L. W. 1997, ApJ, 488, 499
Lemen, J. R., Title, A. M., Akin, D. J., et al. 2012, SoPh, 275, 17
Lin, R. P., Dennis, B. R., Hurford, G. J., et al. 2002, SoPh, 210, 3
Marsh, A. J., Smith, D. M., Glesener, L., et al. 2017, ApJ, 849, 131
Neupert, W. M. 1968, ApJL, 153, L59
Parker, E. N. 1988, ApJ, 330, 474
Parnell, C. E., & Jupp, P. E. 2000, ApJ, 529, 554
Porter, J. G., Toomre, J., & Gebbie, K. B. 1984, ApJ, 283, 879
Shimizu, T. 1995, PASJ, 47, 251
Shimizu, T., & Tsuneta, S. 1997, ApJ, 486, 1045
Tajfirouze, E., & Safari, H. 2012, ApJ, 744, 113
Terzo, S., Reale, F., Miceli, M., et al. 2011, ApJ, 736, 111
Veronig, A. M., Brown, J. C., Dennis, B. R., et al. 2005, ApJ, 621, 482
Walsh, R. W., & Ireland, J. 2003, A&ARv, 12, 1
Wright, P. J., Hannah, I. G., Grefenstette, B. W., et al. 2017, ApJ, 844, 132